

# A Lidar Model for a Rough-Surface Target: Method of Partial Coherence

O. Korotkova,<sup>a</sup> L. C. Andrews,<sup>a</sup> and R. L. Phillips<sup>b</sup>

<sup>a</sup>Department of Mathematics, University of Central Florida, Orlando, FL 32816

E-mail: olga\_korotkova@hotmail.com

landrews@pegasus.cc.ucf.edu

<sup>b</sup>Director, Florida Space Institute, University of Central Florida,

MS: FSI, Kennedy Space Center, FL 32899

E-mail: phillips@mail.ucf.edu

## ABSTRACT

Renewed interest in the propagation characteristics of a partially coherent beam has led to several recent studies that have extended theoretical developments started in the 1970s and 1980s. In this paper we use a model developed by the authors for single-pass propagation of a partially coherent beam and extend it to the case of a Gaussian-beam wave reflected from a finite rough-surface reflecting target. This model can be modeled as a random phase screen (or diffuser) in front of a smooth finite reflector. The target acts like a deep random phase screen for the case of a fully diffuse surface and becomes a continually weakening phase screen as the target surface become smoother. We present mathematical models for the mutual coherence function (MCF) and the scintillation index of the reflected Gaussian-beam wave in the presence of atmospheric turbulence. This analysis includes partial and fully developed speckle from the target. From the normalized MCF, estimates are given for the speckle size in the pupil plane and image plane as a function of transmitted beam wave characteristics, size and roughness of the target, and size of the receiver-collecting lens. Expressions for the scintillation index are valid under weak-to-strong fluctuation conditions and are shown to agree with well-known results in limiting cases of a fully diffuse target and a smooth reflector.

**Key words:** Atmospheric optics, scintillation, rough target, partial coherence, laser radar

## 1. INTRODUCTION

Radar is concerned with the extraction of target information contained in the echo signal. Receiving an echo signal indicates the presence of a target, but target location, velocity, and type of target (i.e., target classification) are also important for applications. The phase of the target-illumination laser beam is distorted by atmospheric turbulence along the propagation path to the target, which is further distorted by the target and then again by atmospheric turbulence along the return path. Because the target surface plays an important role in determining the nature of the echo beam, it is useful to have a mathematical model for certain types of targets in addition to the usual smooth reflector (mirror or retroreflector) or Lambertian (fully diffuse) surface. Because most targets have surfaces that are considered rough on the scale of an optical wavelength, it is useful to model the target surface as partially diffuse, somewhere between the limiting cases of a smooth reflector and a fully diffuse target.

The scattering of light from rough surfaces has been a topic of study for many years [1-3]. Surface roughness is usually defined in terms of surface height deviations from some average value. For random surfaces, it has been customary to start with a Gaussian height model [1], although Stover [3] suggests this may not be necessary. To distinguish between surfaces with the same surface height variations, it is useful to also define a characteristic transverse parameter called the *correlation length*  $l_c$ . The correlation length is typically associated with a model for the surface *auto-correlation function*, which for tractability reasons is also taken in most cases to be a Gaussian function, such as in the Gaussian Schell-model [4]. The Gaussian assumption in the auto-correlation function allows for an easy calculation of the mutual coherence function (MCF), based on the extended Huygens-Fresnel integral [5]. However, the target surface can equally well be characterized by the Fourier transform of the auto-correlation function known as the *power spectral density* (PSD). Use of the PSD has certain computational advantages over the auto-correlation function—in particular, it is possible to develop more general models of surface roughness with the PSD.

Recently, a model for a partially diffuse target has been developed that uses the concepts of a thin phase screen characterized by a PSD, partial coherence, and *ABCD* ray matrices [6,7]. In this paper we review the main results of those studies and then extend some of the work to more general cases.

## 2. MODEL FOR SMOOTH REFLECTOR: FREE SPACE

A schematic for the laser radar system under study is provided in Fig. 1. We illustrate the two-way propagation path in an “unfolded” manner for clarity and characterize the finite target by the combination of a (finite) Gaussian lens and thin phase screen. We will present some results for both the pupil plane of the receiver lens at distance  $2L$  from the transmitter (input plane) and in the focal or detector plane at distance  $L_f$  behind the front receiver lens.

### 2.1 Pupil Plane Analysis

We characterize the propagation path between input plane and the receiver lens (pupil plane) by the *ABCD* ray matrix

$$\begin{aligned} \begin{pmatrix} A_{pp} & B_{pp} \\ C_{pp} & D_{pp} \end{pmatrix} &= \begin{pmatrix} 1 & L \\ 0 & 1 \end{pmatrix} \begin{pmatrix} 1 & 0 \\ i\alpha_R & 1 \end{pmatrix} \begin{pmatrix} 1 & L \\ 0 & 1 \end{pmatrix} \\ &= \begin{pmatrix} 1+i\alpha_R L & L+L(1+i\alpha_R L) \\ i\alpha_R & 1+i\alpha_R L \end{pmatrix}, \end{aligned} \quad (1)$$

where  $\alpha_R$  is a parameter that characterizes the finite size of the target, i.e.,

$$\alpha_R = \frac{2}{kW_R^2}. \quad (2)$$

We assume the transmitted beam wave is a  $TEM_{00}$  collimated Gaussian-beam wave characterized by beam parameters

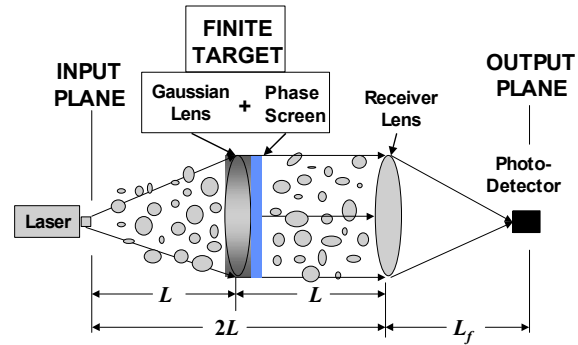


**Figure 1** Schematic of laser radar configuration (unfolded).

$$\Theta_0 = 1, \quad \Lambda_0 = \frac{2L}{kW_0^2}, \quad (3)$$

where  $k$  is optical wave number,  $W_0$  is the beam radius at the exit aperture of the transmitter, and  $L$  is target range. Similarly, the illumination beam is characterized by

$$\Theta_1 = \frac{\Theta_0}{\Theta_0^2 + \Lambda_0^2} = 1 + \frac{L}{F_1}, \quad \Lambda_1 = \frac{\Lambda_0}{\Theta_0^2 + \Lambda_0^2} = \frac{2L}{kW_1^2}, \quad (4)$$

where  $F_1$  and  $W_1$  denote the phase front radius of curvature and spot radius of the illumination beam. Target characteristics will affect the beam properties of the echo beam in the plane of the receiver. Thus, the beam characteristics in the pupil plane are described by beam parameters

$$\begin{aligned} \Theta_2 &= \frac{1 + \bar{\Theta}_1}{(1 + \bar{\Theta}_1)^2 + (\Lambda_1 + \Omega_R)^2} = 1 + \frac{L}{F_2}, \\ \Lambda_2 &= \frac{\Lambda_1 + \Omega_R}{(1 + \bar{\Theta}_1)^2 + (\Lambda_1 + \Omega_R)^2} = \frac{2L}{kW_2^2}, \end{aligned} \quad (5)$$

where  $\bar{\Theta}_1 = 1 - \Theta_1$ ,  $\Omega_R = 2L/kW_R^2$  characterizes the finite size of the target, and  $W_2$  and  $F_2$  denote the beam radius and phase front radius of curvature.

## 2.2 Detector Plane

Let us characterize the (Gaussian) receiver lens by the parameter

$$\alpha_G = \frac{2}{kW_G^2} + i\frac{1}{F_G}, \quad (6)$$

where  $W_G$  is the lens radius and  $F_G$  is its focal length. In this case the overall  $ABCD$  ray matrix describing the entire propagation path to the detector is

$$\begin{aligned} \begin{pmatrix} A_{dp} & B_{dp} \\ C_{dp} & D_{dp} \end{pmatrix} &= \begin{pmatrix} 1 & L_f \\ 0 & 1 \end{pmatrix} \begin{pmatrix} 1 & 0 \\ i\alpha_G & 1 \end{pmatrix} \begin{pmatrix} A_{pp} & B_{pp} \\ C_{pp} & D_{pp} \end{pmatrix} \\ &= \begin{pmatrix} A_{pp} + (C_{pp} + i\alpha_G A_{pp})L_f & B_{pp} + (D_{pp} + i\alpha_G B_{pp})L_f \\ C_{pp} + i\alpha_G A_{pp} & D_{pp} + i\alpha_G B_{pp} \end{pmatrix}. \end{aligned} \quad (7)$$

By using the nondimensional parameter  $\Omega_G = 2L/kW_G^2$  to characterize the finite size of the receiver lens, the beam in the plane of the detector can be described by beam parameters

$$\Theta_3 = \frac{L}{L_f} \left[ \frac{L/L_f - L/F_G + \bar{\Theta}_2}{(L/L_f - L/F_G + \bar{\Theta}_2)^2 + (\Lambda_2 + \Omega_R)^2} \right] = 1 + \frac{L}{F_3},$$

$$\Lambda_3 = \frac{L}{L_f} \left[ \frac{\Lambda_2 + \Omega_R}{(L/L_f - L/F_G + \bar{\Theta}_2)^2 + (\Lambda_2 + \Omega_R)^2} \right] = \frac{2L}{kW_3^2},$$
(8)

where  $\bar{\Theta}_2 = 1 - \Theta_2$ ,  $F_3$  is the phase front radius of curvature, and  $W_3$  is the spot size radius of the beam at the detector. However, the image plane (detector plane) is defined by  $L/L_f - L/F_G + \bar{\Theta}_2 = 0$ , which reduces these parameters to

$$\Theta_3 = 0, \quad \Lambda_3 = \frac{L}{(\Lambda_1 + \Omega_G)L_f}.$$
(9)

### 3. STATISTICAL MODEL FOR ROUGH TARGET: FREE SPACE

We now consider the case where the target surface is not smooth and model the rough surface by a combination of Gaussian lens and thin phase screen as shown in Fig. 1. For the sake of comparison with results deduced from the Gaussian Schell-model, we will assume the power spectrum for the thin phase screen is a Gaussian model described by

$$\Phi_s(\kappa) = \frac{\langle n_1^2 \rangle l_c^3}{8\pi\sqrt{\pi}} \exp\left(-\frac{1}{4}l_c^2\kappa^2\right),$$
(10)

where  $l_c$  is the lateral correlation length of the surface and  $\langle n_1^2 \rangle$  represents the index of refraction fluctuations caused by the screen.

#### 3.1 MCF in the Pupil Plane

In the plane of the receiver, the model for the optical field is given by [8]

$$U_0(\mathbf{r}, 2L) = \frac{1}{A_{pp} + i\alpha_0 B_{pp}} \left( \frac{2\sqrt{\pi}\beta}{k} \right) \exp(2ikL) \exp\left[-\frac{1}{2} \left( \frac{\alpha_0 D_{pp} - iC_{pp}}{A_{pp} + i\alpha_0 B_{pp}} \right) kr^2\right] \exp[\Psi_s(\mathbf{r})],$$
(11)

where  $\beta$  is a constant (see below),  $\Psi_s(\mathbf{r})$  is the random complex phase perturbation induced by the phase screen, and

$$\alpha_0 = \frac{2}{kW_0^2}.$$
(12)

The MCF is defined by the ensemble average  $\Gamma_2^0(\mathbf{r}_1, \mathbf{r}_2, 2L) = \langle U_0(\mathbf{r}_1, 2L)U_0^*(\mathbf{r}_2, 2L) \rangle$ , which requires the evaluation of

$$\langle \exp[\Psi_s(\mathbf{r}_1) + \Psi_s^*(\mathbf{r}_2)] \rangle = \exp \left\{ -4\pi^2 k^2 \Delta z \int_0^\infty \kappa \Phi_s(\kappa) \left[ 1 - \exp \left( -\frac{\Lambda_2 L \kappa^2}{k} \right) J_0(\kappa |\Theta_2 \mathbf{p} - 2i\Lambda_2 \mathbf{r}|) \right] d\kappa \right\}, \quad (13)$$

where  $\Delta z$  is the thickness of the screen. It has been shown that this evaluation leads to the MCF [6,7]

$$\begin{aligned} \Gamma_2^0(\mathbf{r}, \mathbf{p}, 2L) &= \frac{4\pi\beta^2 (\Theta_1^2 + \Lambda_1^2) (\Theta_2^2 + \Lambda_2^2)}{k^2 (1 + 4q_c \Lambda_2)} \exp \left[ -\left( \frac{\Lambda_2}{1 + 4q_c \Lambda_2} \right) \frac{kr^2}{L} \right] \\ &\times \exp \left[ -\frac{1}{(1 + 4q_c \Lambda_2)} \left( \frac{\Lambda_2}{4} + (\Theta_2^2 + \Lambda_2^2) q_c \right) \frac{k\rho^2}{L} \right] \exp \left[ -\left( \frac{1 - \Theta_2 + 4q_c \Lambda_2}{1 + 4q_c \Lambda_2} \right) \frac{ik}{L} \mathbf{r} \cdot \mathbf{p} \right]. \end{aligned} \quad (14)$$

Here we are introducing the vectors  $\mathbf{r} = (\mathbf{r}_1 + \mathbf{r}_2)/2$  and  $\mathbf{p} = \mathbf{r}_1 - \mathbf{r}_2$ , and set  $\rho = |\mathbf{p}|$ . Also, we now define  $\beta^2 = k^2/4\pi$  for smooth targets and  $\beta^2 = T_0^2/\pi l_c^2$  for fully diffuse or Lambertian targets ( $l_c \rightarrow 0$ ), where  $T_0^2$  is the reflection coefficient. Last, we have introduced the nondimensional ‘‘roughness’’ parameter

$$q_c = \frac{L}{kl_c^2}. \quad (15)$$

Note that the form of the MCF (14) is similar to that for a smooth target obtained in the limit  $l_c \rightarrow \infty$ , viz.,

$$\begin{aligned} \Gamma_2^0(\mathbf{r}, \mathbf{p}, 2L) &= (\Theta_1^2 + \Lambda_1^2) (\Theta_2^2 + \Lambda_2^2) \exp \left( -\Lambda_2 \frac{kr^2}{L} \right) \\ &\times \exp \left( -\Lambda_2 \frac{k\rho^2}{4L} \right) \exp \left[ -(1 - \Theta_2) \frac{ik}{L} \mathbf{r} \cdot \mathbf{p} \right]. \end{aligned} \quad (16)$$

The first exponential function in (16) describes the profile of the mean irradiance in free space reflected from a smooth surface and can therefore be used to infer beam size  $W_2$ . For a partially coherent beam reflected from a rough surface, the first exponential function in (14) can similarly be used to define the increased beam size caused by the diffuser, i.e.,

$$W_{2d} = W_2 (1 + 4q_c \Lambda_2). \quad (17)$$

The coherence properties of the beam can be inferred from the magnitude of the complex degree of coherence defined by

$$|\gamma_s(\rho, 2L)| = \frac{|\Gamma_2^0(\mathbf{r}_1, \mathbf{r}_2, 2L)|}{\sqrt{\Gamma_2^0(\mathbf{r}_1, \mathbf{r}_1, 2L)\Gamma_2^0(\mathbf{r}_2, \mathbf{r}_2, 2L)}} = \exp \left[ -\frac{1}{2} D_s(\rho, 2L) \right], \quad (18)$$

which reduces to

$$|\gamma_s(\rho, 2L)| = \exp\left[-\left(\frac{\Theta_2^2 + \Lambda_2^2}{1 + 4q_c \Lambda_2}\right) \frac{\rho^2}{l_c^2}\right] = \exp\left(-\frac{\rho^2}{\rho_{pp, speckle}^2}\right). \quad (19)$$

From the last expression in (19), we can define the speckle radius in the pupil plane by

$$\rho_{pp, speckle} = \sqrt{\frac{(1 + 4q_c \Lambda_2) l_c^2}{\Theta_2^2 + \Lambda_2^2}}. \quad (20)$$

In the limit of a fully diffuse target ( $l_c \rightarrow 0$ ), we have  $\Lambda_2 / (\Theta_2^2 + \Lambda_2^2) \rightarrow \Lambda_1 + \Omega_R$ , and consequently

$$\rho_{pp, speckle} = \sqrt{\frac{\lambda L (\Lambda_1 + \Omega_R)}{\pi}} = \frac{\sqrt{2} \lambda L}{\pi W_R} \sqrt{1 + \frac{W_R^2}{W_1^2}}. \quad (21)$$

Equations (20) and (21) are more general than Goodman's classic result [9] because they involve the partial coherence of the target and the illumination beam as well as target size. However, in the case of an unresolved target ( $W_R \ll W_1$ ), Eq. (21) simplifies to Goodman's result, viz.,

$$\rho_{pp, speckle} = \frac{\sqrt{2} \lambda L}{\pi W_R}, \quad (\text{unresolved target}). \quad (22)$$

A related quantity used in accessing lidar performance is the number of speckle cells  $N_s$  captured by the receiver telescope [10,11]. Based on (22), the number of speckle cells on the receiver lens is

$$N_s = 1 + \frac{S_{lens}}{S_{speckle}} = \frac{1 + 2\Omega_G \Omega_R}{2\Omega_G \Omega_R}, \quad (\text{unresolved target}) \quad (23)$$

where  $S_{lens}$  and  $S_{speckle}$  denote the receiver aperture area and speckle correlation area, respectively. In the limiting case of small target and/or small receiver lens, we have  $\Omega_G \Omega_R \rightarrow \infty$  and the number of speckle cells reduces to one.

### 3.2 MCF in the Detector Plane

In the plane of the detector we will calculate only the speckle size based on the modulus of the complex degree of coherence as defined by Eq. (18) for the pupil plane. It has been shown that the wave structure function leads to [6]

$$D_s(\mathbf{r}_1, \mathbf{r}_2, 2L + L_f) = 4\pi^2 k^2 \Delta z \operatorname{Re} \int_0^\infty \kappa \Phi_s(\kappa) \exp\left[-\frac{L(\Theta_2^2 + \Lambda_2^2 \Omega_G) \kappa^2}{k(\Lambda_2 + \Omega_G)}\right] \\ \times \left\{ I_0 \left[ \frac{2L\Theta_2 r_1 \kappa}{L_f(\Lambda_2 + \Omega_G)} \right] + I_0 \left[ \frac{2L\Theta_2 r_2 \kappa}{L_f(\Lambda_2 + \Omega_G)} \right] - 2J_0 \left[ \kappa \left| \frac{L\Lambda_2 \mathbf{p}}{L_f(\Lambda_2 + \Omega_G)} + \frac{2iL\Theta_2 \mathbf{r}}{L_f(\Lambda_2 + \Omega_G)} \right| \right] \right\} d\kappa, \quad (24)$$

from which we deduce

$$|\gamma(\rho, 2L + L_f)| = \exp\left\{-\frac{L^2(\Theta_2^2 + \Lambda_2^2)}{L_f^2(\Lambda_2 + \Omega_G)[\Lambda_2 + \Omega_G + 4(\Theta_2^2 + \Lambda_2\Omega_G)q_c]}\left(\frac{\rho^2}{l_c^2}\right)\right\}. \quad (25)$$

Hence, the speckle size in the detector plane implied by this expression is

$$\rho_{speckle, dp} = \sqrt{\frac{L_f^2(\Lambda_2 + \Omega_G)[\Lambda_2 + \Omega_G + 4(\Theta_2^2 + \Lambda_2\Omega_G)q_c]}{L^2(\Theta_2^2 + \Lambda_2^2)}}. \quad (26)$$

In the limit of a fully diffuse surface we obtain

$$\rho_{speckle, dp} = 1.27\left(\frac{\lambda L_f}{D_G}\right)\sqrt{1 + \Omega_G\Omega_R} \quad (\text{unresolved target}). \quad (27)$$

#### 4. STATISTICAL MODEL FOR ROUGH TARGET: ATMOSPHERE

Here we assume that atmospheric turbulence is statistically independent of the fluctuations associated with the rough target. Also, the summary below of previous results is for only the pupil plane of the receiver.

The modulus of the complex degree of coherence (18) now takes the form

$$|\gamma_s(\rho, 2L)| = \exp\left[-\frac{1}{2}D_{atm}(\rho, 2L) - \frac{1}{2}D_s(\rho, 2L)\right], \quad (28)$$

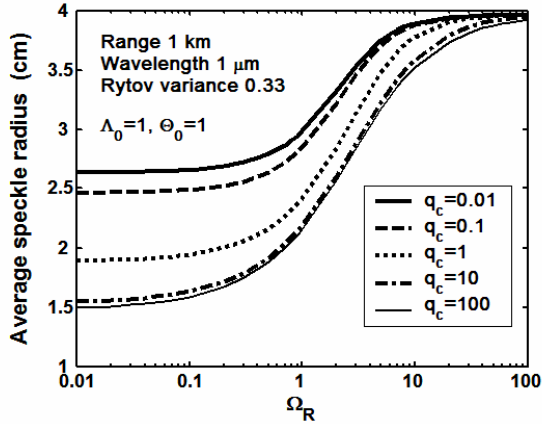


**Figure 2** Average speckle size of the return wave in the pupil plane of the receiver.

parameter  $q_c$ . We assume the incident beam is collimated ( $\Theta_0 = 1$ ) with  $\Lambda_0 = 1$ . The propagation distance

where we have included the wave structure function (WSF) for the atmosphere which we write in general in the form  $D_{atm}(\rho, 2L) = 2(\rho/\rho_0)^{5/3}$ . The parameter  $\rho_0$  is the spatial coherence radius of the coherent beam in atmospheric turbulence [8]. By using the approximation  $(\rho/\rho_0)^{5/3} \approx (\rho/\rho_0)^2$ , the implied speckle size of the partially coherent beam can be expressed as

$$\rho_{pp, speckle} \approx \left[ \left( \frac{\Theta_2^2 + \Lambda_2^2}{1 + 4q_c\Lambda_2} \right) \frac{\rho^2}{l_c^2} + \frac{1}{\rho_0^2} \right]^{-1/2} \quad (29)$$

(unresolved target)

The average speckle radius (29) is shown in Fig. 2 as a function of normalized target size  $\Omega_R$  and several values of roughness

is taken to be  $L = 1$  km, wavelength  $\lambda = 1$   $\mu\text{m}$ , and the Rytov variance is assumed to be in the weak fluctuation regime. In the limit of small reflectors ( $\Omega_R \gg 1$ ), all curves saturate at the same level, but the target roughness plays a role in the speckle size for the case of larger targets ( $\Omega_R < 1$ ).

In the limiting case of a fully diffuse target, we find that (29) reduces to

$$\rho_{pp, \text{speckle}} = \frac{\sqrt{2} \lambda L / \pi W_R}{\sqrt{1 + 2(\lambda L / \pi W_R \rho_0)^2}}, \quad (\text{unresolved target}) \quad (30)$$

from which we deduce the average number of speckle cells

$$N_s = 1 + \frac{S_{\text{lens}}}{S_{\text{speckle}}} = \frac{1 + 2\Omega_G \Omega_R + 2(\lambda L / \pi W_R \rho_0)^2}{2\Omega_G \Omega_R}, \quad (\text{unresolved target}). \quad (31)$$

Hence, we see that the average speckle size (30) is reduced in the presence of atmospheric turbulence provided the spatial coherence radius  $\rho_0 < \lambda L / \pi W_R$ . Otherwise, atmospheric turbulence will not change the speckle size and average number of speckle cells.

In the case of a resolved target, it has been shown that the average speckle size is [6]

$$\rho_{pp, \text{speckle}} \approx \frac{\lambda L}{\pi W_R} \sqrt{\frac{1 + W_R^2 / W_1^2}{1 + (1 + W_R^2 / W_1^2) (\lambda L / \pi W_R \rho_0)^2}}, \quad (\text{resolved target}) \quad (32)$$

and the corresponding number of speckle cells is

$$N_s = 1 + \frac{S_{\text{lens}}}{S_{\text{speckle}}} = \frac{1 + \Omega_G \Omega_R + (1 + W_R^2 / W_1^2) (\lambda L / \pi W_R \rho_0)^2}{\Omega_G \Omega_R (1 + W_R^2 / W_1^2)}, \quad (\text{resolved target}). \quad (33)$$

Both of these expressions are dependent once again on using the approximation  $(\rho / \rho_0)^{5/3} \approx (\rho / \rho_0)^2$ .

## 5. SCINTILLATION INDEX

In developing expressions for the scintillation index in the pupil plane of the receiver, we will consider only the case of an incident *spherical wave* under weak fluctuation conditions. Also, we will consider the response time of the detector  $\tau_d$  and the coherence time of the target surface  $\tau_s$  caused by temporal variations of the surface. To begin, we will consider the surface in the absence of atmospheric turbulence.

### 5.1 Fast Detector Case: Free-Space Propagation

If the coherence time of the detector is much shorter than the coherence time of the rough target surface (i.e., if  $\tau_d \ll \tau_s$ ), the detector will be sensitive to intensity fluctuations of the target. In this case, the phase screen model leads to the (on-axis) scintillation index defined by

$$\sigma_{I,\text{diff}}^2(2L) = 8\pi^2 k^2 \Delta z \int_0^\infty \kappa \Phi_s(\kappa) e^{-\Lambda_2 L \kappa^2 / k} \left[ 1 - \cos\left(\frac{\Theta_2 L \kappa^2}{k}\right) \right] d\kappa, \quad (34)$$

which, by use of the Gaussian spectrum (10), yields

$$\sigma_{I,\text{diff}}^2(2L) = 1 - \frac{(1 + 4\Lambda_2 q_c)^2}{(1 + 4\Lambda_2 q_c)^2 + 16q_c^2 \Theta_2^2}. \quad (35)$$

Limiting cases of (35) lead to  $\sigma_{I,\text{diff}}^2(2L) = 0$  for a weak diffuser ( $l_c \rightarrow \infty$ ) and to  $\sigma_{I,\text{diff}}^2(2L) = 1$  for a strong diffuser ( $l_c \rightarrow 0$ ).

## 5.2 Slow Detector: Effective Beam Parameters

For a smooth target reflecting surface, we can use beam parameters (5) to define beam characteristics of the return wave in free space. For a rough target, the “effective” Gaussian beam can be characterized by the “effective beam parameters” [7]

$$\Theta_{2e} = \frac{\Theta_2}{1 + 4\Lambda_2 q_c}, \quad \Lambda_{2e} = \frac{\Lambda_2 [1 + 4q_c / (\Lambda_1 + \Omega_R)]}{1 + 4\Lambda_2 q_c}, \quad (36)$$

deduced from the MCF (14) by comparison with the smooth surface MCF (16). Under weak fluctuation conditions in a bistatic configuration, the resulting (on-axis) scintillation index is [7]

$$\sigma_{I,\text{atm}}^2(0,2L) = 7.72 \sigma_1^2 \text{Re} \left\{ i^{5/6} {}_2F_1 \left( -\frac{5}{6}, \frac{11}{6}; \frac{17}{6}; 1 - \Theta_{2e} + i\Lambda_{2e} \right) - \frac{11}{16} \Lambda_{2e}^{5/6} \right\}, \quad (37)$$

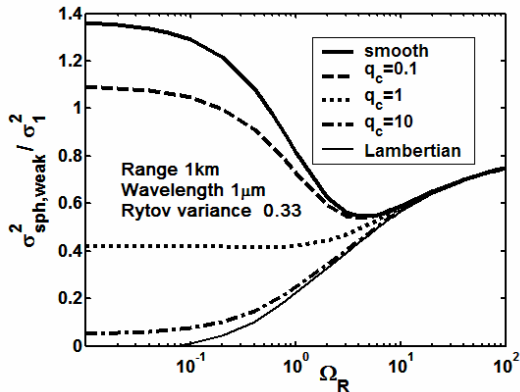


**Figure 3** Scaled scintillation index of a reflected spherical wave from a partially diffuse target.

where  $\text{Re}$  denotes the real part and  ${}_2F_1$  denotes a hypergeometric function. We plot (37) in Figure 3 as a function of normalized target size  $\Omega_R$  and several partially diffuse targets ranging from a smooth reflector to a fully diffuse (or Lambertian) target. For small targets ( $\Omega_R \gg 1$ ), all curves merge to the same scintillation index, but for large targets ( $\Omega_R \ll 1$ ), each curve saturates to a certain level depending on the normalized surface correlation length  $q_c$ .

## 5.3 Integrated Intensity

The integrated intensity can be represented by  $E(\mathbf{r}, 2L) = \frac{1}{T} \int_{-T}^T I(\mathbf{r}, 2L; t) dt$ , where  $I(\mathbf{r}, 2L; t)$  is

the instantaneous intensity and  $T$  is the integration time. From linear system analysis, we recognize  $E(\mathbf{r}, 2L)$  as the output of an ideal integrator with impulse response function given by

$h(t) = (1/T)U(T-|t|)$ , where  $U(t)$  is the unit step function. The corresponding system function is  $H(\omega) = (\sin \omega T/2)/(\omega T/2)$ , which is the Fourier transform of  $h(t)$ . From linear systems theory, it is known that the variance function of the output is related to the covariance function of the input by

$$\sigma_E^2(2L) = \sigma_{I,\text{diff}}^2(2L) \left[ \frac{1}{T} \int_{-T}^T \left(1 - \frac{|\tau|}{T}\right) |\gamma(\tau)|^2 d\tau \right], \quad (38)$$

where  $|\gamma(\tau)|^2$  is the normalized temporal covariance function of the instantaneous source intensity. In arriving at (38), we have divided by the square of the mean intensity to obtain the scintillation index and we have assumed the covariance function of the input can be expressed as a product of the spatial covariance and temporal covariance. It is interesting that the above integral yields similar values for various models of  $|\gamma(\tau)|^2$ , e.g., (38) produces roughly the same results for either a Gaussian or Lorentzian spectrum [12]. If we use a Lorentzian spectrum model, for example, it follows that  $\gamma(\tau) = e^{-|\tau|/T}$ , and in this case we can replace the time period  $T$  in (38) with the response time of the detector  $\tau_d$ . The result of doing so leads to the analytic expression

$$\sigma_E^2(2L) = \sigma_{I,\text{diff}}^2(2L) \left[ \frac{\tau_s}{\tau_d} + \frac{1}{2} \left( \frac{\tau_s}{\tau_d} \right)^2 \left( e^{-2\tau_d/\tau_s} - 1 \right) \right]. \quad (39)$$

Equation (39) gives us the scintillation index of the integrated intensity as a function of coherence time of the target source and response time of the detector. The two limiting cases of a slow and fast detector are readily deduced from (39), which yields

$$\sigma_E^2(2L) = \begin{cases} \sigma_{I,\text{diff}}^2(2L), & \tau_d \ll \tau_s \\ \frac{\tau_s}{\tau_d} \sigma_{I,\text{diff}}^2(2L), & \tau_d \gg \tau_s \end{cases}. \quad (40)$$

In the lower expression (slow detector case), the ratio  $\tau_s/\tau_d$  approaches zero, which eliminates all intensity fluctuations associated with the diffuser alone.

#### 5.4 Fast Detector Case: Atmospheric Effects

By following the technique used in Ref. 13 for taking into account surface roughness irregularities, we express the instantaneous (normalized) intensity as  $I = EI_{\text{atm}}$ , where  $E$  is the integrated intensity of the source and  $I_{\text{atm}}$  is the random intensity due to the atmosphere and diffuser. Hence, we find  $\langle I \rangle = \langle E \rangle \langle I_{\text{atm}} \rangle = 1$ ,  $\langle I^2 \rangle = \langle E^2 \rangle \langle I_{\text{atm}}^2 \rangle = (1 + \sigma_E^2)(1 + \sigma_{I,\text{atm}}^2)$ , and the scintillation index takes the form

$$\sigma_I^2(2L) = \frac{\langle I^2 \rangle}{\langle I \rangle^2} - 1 = \sigma_{I,\text{atm}}^2 + \sigma_E^2 \left( 1 + \sigma_{I,\text{atm}}^2 \right), \quad (41)$$

where  $\sigma_E^2$  is defined by (39) and  $\sigma_{I,\text{atm}}^2$  is the scintillation index of the atmosphere and diffuser (37).

In Figs. 4-6 we plot the scintillation index (41) as a function of normalized target size  $\Omega_R$  for different surface correlation widths and different ratios  $\tau_s/\tau_d = 0.1, 1, 10$ . The case  $\tau_s/\tau_d = 0.1$  illustrated in Fig. 4 corresponds to a slow detector whereas the case  $\tau_s/\tau_d = 10$  shown in Fig. 6 corresponds to a fast detector. Here we see that the combination of target size and coherence ratios has a significant effect on the implied scintillation index, particularly for large targets ( $\Omega_R \ll 1$ ). In all cases the smooth target leads to the same scintillation index.

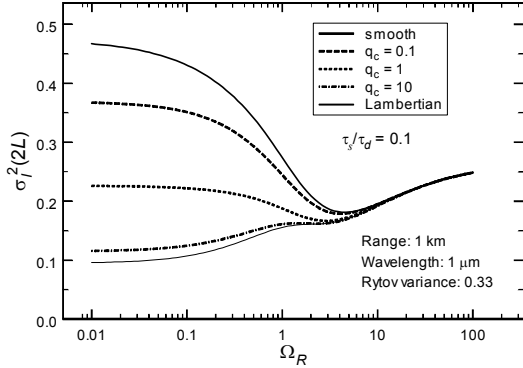


**Figure 4** Scintillation index of a reflected spherical wave from a partially diffuse surface with  $\tau_s / \tau_d = 0.1$ .

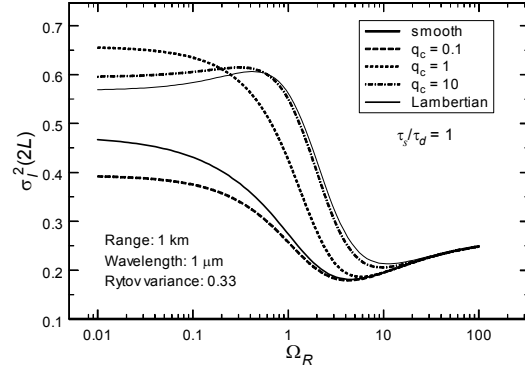


**Figure 5** Same as Figure 4 with  $\tau_s / \tau_d = 1$ .

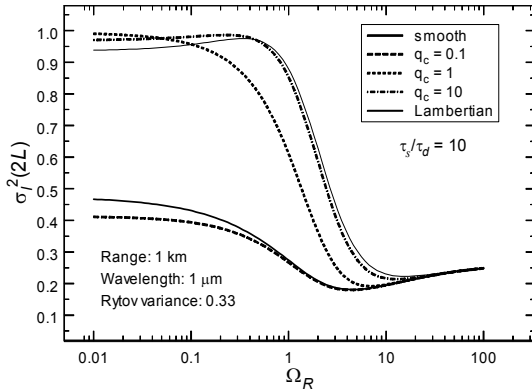


**Figure 6** Same as Figure 4 with  $\tau_s / \tau_d = 10$ .

a more conventional Gaussian Schell-model. However, by the use of  $ABCD$  ray matrices and our model we have also obtained estimates of the speckle size and number of speckle cells in the plane of the detector. Moreover, we have obtained expressions for the scintillation index for cases ordinarily characterized as “fast detector” or “slow detector” cases. In all cases we assume that surface height fluctuations are sufficiently large that the phase variance of the reflected wave is also large (much more than  $2\pi$  radians). In such cases the phase lateral correlation length is directly related to the lateral correlation length of the surface heights [14].

In the fast detector case illustrated in Fig. 6 it is interesting to observe the contrast between relatively smooth targets ( $q_c \leq 0.1$ ) and fairly rough targets ( $q_c \geq 1$ ) when the target size is large. Namely, the large rough targets have scintillation index on the order of unity corresponding to a fully diffuse target.

## 6. SUMMARY

The model developed here and in previous papers [6,7] based on a thin phase screen model for a target with rough surface characterized by its transverse correlation length has been shown to give the same results for the MCF, speckle size, and number of speckle cells in the pupil plane as those obtained with

## 7. REFERENCES

- [1] P. Beckmann and A. Spizzichino, *The Scattering of Electromagnetic Waves from Rough Surfaces* (Pergamon, New York, 1963).
- [2] J. A. Ogilvy, *Theory of Wave Scattering from Random Rough Surfaces* (Adam Hilger, Bristol, 1991).
- [3] J. C. Stover, *Optical Scattering* (SPIE Optical Engineering Press, Bellingham, 1995).
- [4] A. C. Schell, *The Multiple Plate Antenna* (Doctoral Dissertation, Massachusetts Institute of Technology, Cambridge, 1961).
- [5] L. Mandel and E. Wolf, *Optical Coherence and Quantum Optics* (Cambridge University Press, Cambridge, 1995).
- [6] O. Korotkova and L. C. Andrews, "Speckle propagation through atmospheric turbulence: effects of partial coherence of the target, Proc. SPIE **4723**, 73-84 (2002).
- [7] O. Korotkova, L. C. Andrews, and R. L. Phillips, "Laser radar in turbulent atmosphere: effect of target with arbitrary roughness on second- and fourth-order statistics of a Gaussian beam," Proc. SPIE **5086** (2003).
- [8] L. C. Andrews and R. L. Phillips, *Laser Beam Propagation through Random Media* (SPIE Optical Engineering Press, Bellingham, 1998).
- [9] J. W. Goodman, "Statistical properties of laser speckle patterns," Chap. 2 in *Laser Speckle and Related Phenomenon*, J. C. Dainty, ed. (Springer, Verlag, Berlin, 1975).
- [10] A. Dabas, P. H. Flamant, and P. Salamitou, "Characterization of pulsed coherent Doppler lidar with the speckle effect," Appl. Opt. **33**, 6524-6532 (1994).
- [11] P. Drobinski, A. M. Dabas, P. Delville, P. H. Flamant, J. Pelon, and R. M. Hardesty, "Refractive-index structure parameter in the planetary boundary layer: comparison of measurements taken with a 10.6- $\mu\text{m}$  coherent lidar, a 0.9- $\mu\text{m}$  scintillometer, and *in situ* sensors," Appl. Opt. **38**, 1648-1656 (1999).
- [12] J. W. Goodman, *Statistical Optics* (Wiley, New York, 1985).
- [13] L. C. Andrews, R. L. Phillips, and C. Y. Hopen *Laser Beam Scintillation with Applications* (SPIE Optical Engineering Press, Bellingham, 2001).
- [14] H. T. Yura, S. G. Hanson, and L. Lading, "Laser Doppler velocimetry: analytical solution to the optical system including the effects of partial coherence of the target," J. Opt. Soc. Am. A **12**, 2040-2047 (1995).